The 12th International Symposium on Transport Phenomena and Dynamics of Rotating Machinery
Honolulu, Hawaii, February 17-22, 2008

ISROMAC12-2008-20044

EXPERIMENTAL AND NUMERICAL INVESTIGATIONS OF THE RADIAL THRUST IN A CENTRIFUGAL PUMP

J.F. Combes[1], A. Boyer[1], L. Gros[2], D. Pierrat[2], G. Pintrand[2], P. Chantrel[3]

[1]EDF R&D, 6 quai Watier 78400 Chatou, France, +33 1 3087 7244
jean-francois.combes@edf.fr, alain.boyer@edf.fr
[2]CETIM, 74 route de la Jonelière, 44000 Nantes, France, +33 2 4037 3635,
laurent.gros@cetim.fr, daniel.pierrat@cetim.fr, guillaume.pintrand@cetim.fr
[3]ALSTOM Bergeron CERG, rue Lavoisier, 38800 Le Pont de Claix, France, +33 4 7640 9040
paul.chantrel@power.alstom.com

ABSTRACT

In order to determine the static and dynamic loads in rotating machinery, a specific biconical hydrostatic bearing was devised. Static and dynamic pressures are measured in eight cells allowing to obtain the axial and radial forces and momentum.

This bearing was used to measure the axial and radial thrust in a centrifugal pump for different operating conditions including cavitation or entrained air.

The flow within the whole pump, including the inlet pipe, the impeller, the volute and the exhaust pipe was calculated for 5 flowrates, ranging from 0.4 Qn to 1.2 Qn. For the nominal and the lowest flowrates, a comparison was made between a full unsteady calculation and frozen rotor ones for 3 positions. For the other flowrates, a frozen rotor model was chosen. The radial thrusts obtained are in a good agreement with the experimental ones for each flowrate.

INTRODUCTION

In centrifugal pumps the impellers are subject to radial forces which can be split between a static part, the radial thrust, a rotating and a fluctuating one. The rotating part consists in an hydraulic unbalance which can be due to geometrical non uniformities of the impeller. The fluctuating part is mainly linked to the interactions between the blades an the fixed parts such as the volute tongue, while the radial thrust is essentially due to the non uniform pressure distribution around the impeller due to the volute. It presents a minimum value at a flowrate Qv for which the flow presents a null incidence at the tongue. Generally, Qv is close to Qn. The radial thrust direction depends also on the flowrate and is reversed at Qv. Generally, the radial thrust is determined experimentally by using some specific devices such as strain gauges mounted on the shaft, or by integration of the measured pressure field around the impeller. These experiments have led to empirical formulas such as

$$F_r = k_r \rho g H d_2 b_2 \quad with \quad k_r = k_{r0}\left[1-\left(Q/Qv\right)^2\right],$$

k_{r0} being the radial thrust coefficient at shut-off.

With the development of highly efficient CFD codes, it is now possible to calculate simultaneously the flow in the whole impeller and in the volute. Such calculations have been presented for instance by Asuaje et al. (2005), Baun and Flack (2002), Gonzalez et al. (2002), Kaupert (2002), Majidi and Siekmann (2000) or Treutz and Hansen (2002).

By integration of the pressure field and the viscous stresses on the impeller, one can access to the unsteady forces and particularly to the radial thrust and to the fluctuating radial forces. We present here such a calculation for a centrifugal pump for which experimental results were available at different flowrates. We present also the specific instrumentation which was developed for this use and especially for the cases where flow simulation is not yet available such as unsteady cavitation or air passage.

NOMENCLATURE

BEP :	best efficiency point
b2 :	impeller outlet channel width (m)
d2 :	impeller outlet diameter (m)
Fr :	radial thrust (N)
H :	head (m)
N :	rotational speed (rpm)
Q :	flowrate (m3/s)
Qn :	flow at BEP
Qv :	flow at minimum radial thrust
P :	power (W)

EXPERIMENTAL SET-UP

Test loop

The tests have been performed using the EPOCA closed test loop, designed to study cavitation in pumps and valves. It uses a variable speed motor of 330 kW, with a rotational speed from 360 to 3600 rpm. The inlet pressure can be varied from 0.2 to 4 bar.

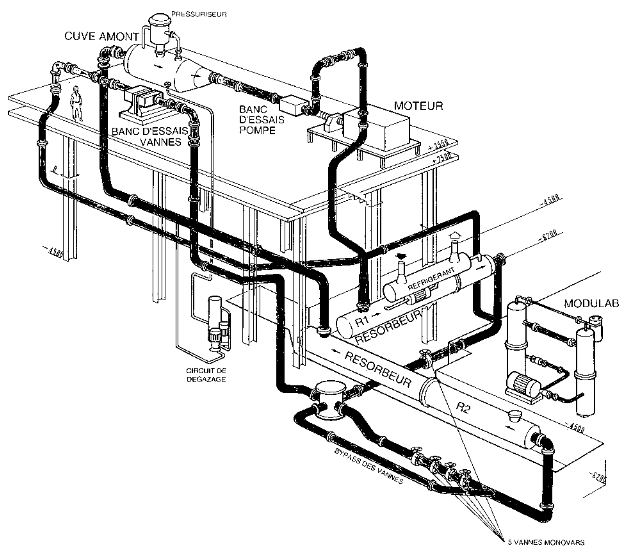

Figure 1 : EPOCA test rig

Hydrostatic bearing

In order to determine the static and dynamic stresses in rotating machinery, a specific bearing was devised (Chantrel et al., 2004). It was designed on the basis of a double conical hydrostatic bearing fed by a high-pressure pump. The bearing includes eight cavities (figure 2) in which static pressure taps and piezoelectric sensors are fitted. This sensors provide static pressure fluctuation information in each cavity with a frequency range from 1 Hz to 30 kHz and a pressure range from 10 Pa to 5 10^7 Pa. Six differential pressure transducers are used in order to obtain the force and the moment components : for a fluid supply of 45 bar, the maximum loads are the following :

− axial force Fx : 37 000 N
− radial force Fy and Fz : 62 000 N
− moment My and Mz : 7 500 Nm
- maximum frequency : 500 Hz

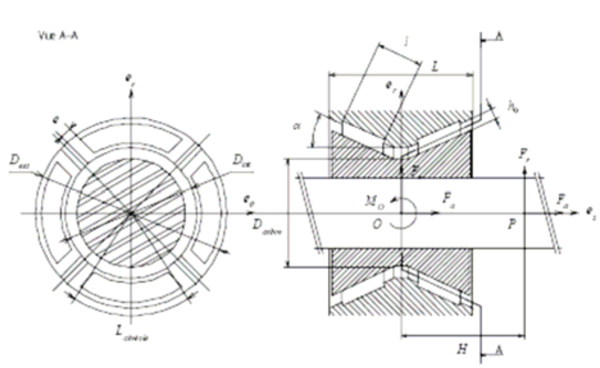

Figure 2 : Hydrostatic bearing principle

The relationship between forces, moments and pressures can be found from geometric areas and they have been verified by calibration. Due to the high value of its stiffness, such a device presents the advantage of a high frequency pass-band for measuring forces or moment fluctuations.

This bearing was used to measure the axial and radial thrust in a centrifugal pump for different operating conditions including cavitation or entrained air. Figure 3 shows the mounting of the bearing on a centrifugal pump.

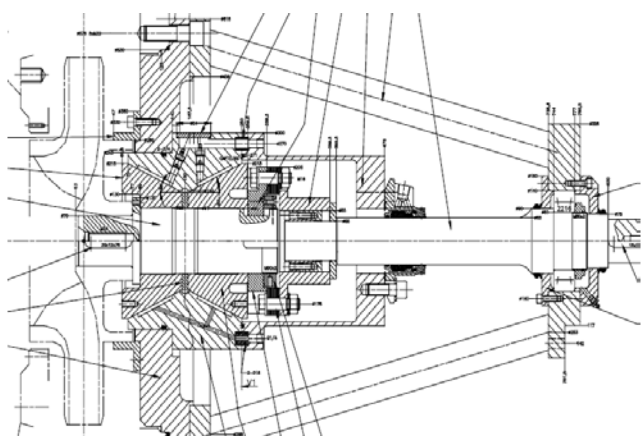

Figure 3 : Implementation of the bearing

Pump

The measurements were performed on a Gourdin LE200-500 centrifugal pump. Some modifications were made on this pump : blades trimmed to a diameter of 0.445 m from an initial value of 0.5 m, and modifications brought to the volute in order to allow visualizations and the mounting of the hydrostatic bearing.

Its main characteristics are :

- volute pump with a six-blade impeller,
- BEP at N = 1450 rpm : Q_n = 0.194 m3/s (700 m3/h) , H_n = 62 m, P_n = 140 kW, η_n = 0.85, n_q = 29
- inlet diameter : 0.2349 m, outlet diameter : 0.445 m, inlet volute diameter : 0.52 m

The radial thrust measured on this pump with the hydrostatic bearing is plotted on figure 4 as a function of the flow rate showing the classical V-shape. One can notice than the minimum thrust value is obtained at a low flow (500 m3/h) compared to the BEP. On figure 5 one can see an example of force fluctuations due to the interaction between the blades and the volute tongue.

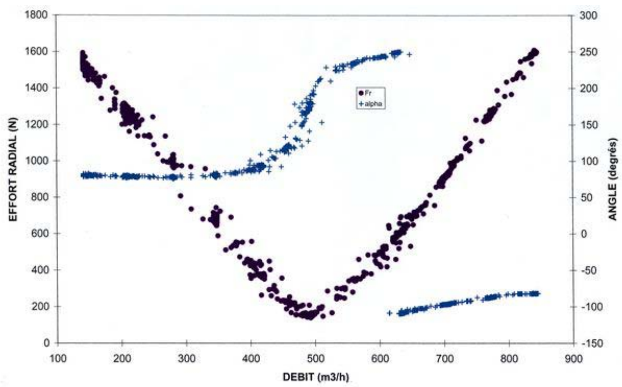

Figure 4 : Radial thrust and direction measured

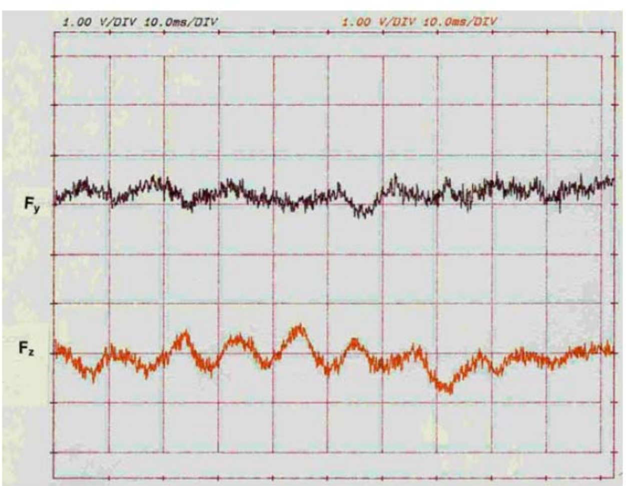

Figure 5 : Example of radial forces fluctuations due to the interaction between the blades and the volute

NUMERICAL STUDY

Flow simulation

The flow in the pump was simulated with the finite volume CFD software ANSYS CFX-TASCflow v.2.12. The ensemble-averaged conservation equations for mass and momentum are solved together with the Shear Stress Transport turbulence model (SST). This model uses a combination of the k-ε model for the core flow and the k-ω one for near wall regions.

For coupling the stationary (inlet pipe and volute) and rotating regions (impeller), this software allows different options. In this study we used at first the frozen rotor model in which the flow in the stationary and rotating regions are calculated at a fixed circumferential position for the impeller relative to the volute. As the results can depend on this position, for correctness, several simulations must be run with different positions.

We used also the transient rotor-stator option in which all quantities are transferred between the stationary and the rotating frames at each time step, allowing calculation of unsteady interaction phenomena.

Geometry

CAD models for the impeller and for the volute were made using SolidWorks software from 3D measurements. For some parts of the blade which were not directly accessible to the measuring arm, the measurements were made on an impression of the blade.

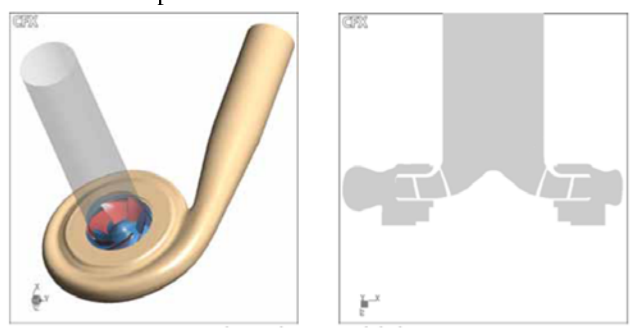

Figure 6 : CAD model of the pump

The balancing holes were not included in the model.

Mesh

The impeller was meshed with ANSYS CFX-Turbogrid v1.6. For the six blades, the whole mesh consists of 420 000 elements (figure 7). The inlet pipe (70 000 elements) and the volute (770 000) elements) were meshed with ICEM CFD. Altogether there were about 1 250 000 elements.

The choice of the final mesh was made after a sensitivity study on the mesh size. Thus, for the impeller alone with one blade passage, meshes from 20 000 to 110 000 elements were tested at the nominal flowrate : the calculations have shown no differences for a mesh greater than 65000 elements, leading to the choice of the final mesh for the whole impeller.

In the same manner, several meshes for the volute were tested, ranging from 300 000 to 770 000 elements.

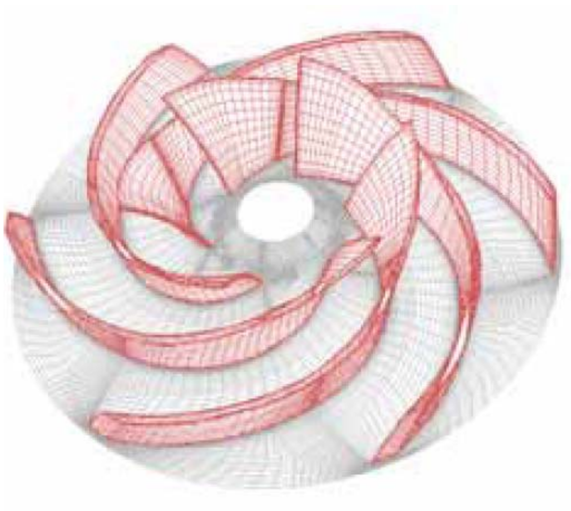

Figure 7 : Surface mesh of the impeller

Calculations

The flow within the whole pump, including the inlet pipe, the impeller, the volute and the exhaust pipe was calculated for 5 flowrates, ranging from 0.43 Qn to 1.2 Qn.

At the lowest and nominal flowrates, the frozen rotor model was used for three positions (figure 8).

Q (m3/h)	300	450	550	700	850
Q/Qn	0.43	0.64	0.79	1.00	1.21
Frozen rotor 1 position		x	x		x
Frozen rotor 3 positions	x			x	
Sliding mesh unsteady	x			x	

Figure 8 : Three impeller positions for the frozen rotor model

Before these calculations a numerical study was done to evaluate their sensibility to numerical and physical parameters such as the mesh density, the time step, the turbulence model (k-ε and k-ω SST), the convergence criteria and the numerical scheme. The best compromise was used for the final calculations.

Unsteady calculations

At the nominal and lowest flow rate, a full unsteady calculation was also made on a mesh consisting of 70 000 elements in the inlet pipe, 360 000 in the impeller and 520 000 in the volute.

The simulation was done for 7 revolutions at Qn with a rotation of 2° of the impeller domain at each time step, leading to a periodic flow in the whole domain (figure 9).

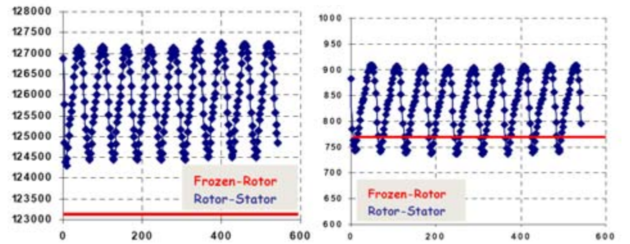

Figure 9 : Power and radial thrust evolution during the 1 ½ last revolution at Qn

At 0.43 Qn, the simulation was done for a little more than 2 revolutions with a rotation of 1° at each time step (figure 10).

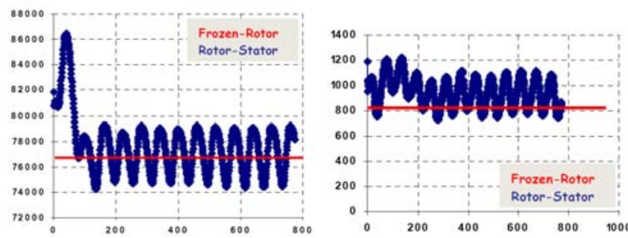

Figure 10 : Power and radial thrust evolution at 0.43 Qn

RESULTS

Overall performances

The evolution of the head, the efficiency and the power as a function of the flowrate is plotted on figure 11. The evolution is well reproduced by the calculations, with slight overestimation of the head and underestimation of the power, leading to too high efficiencies. The mechanical losses were not taken into account in the calculations.

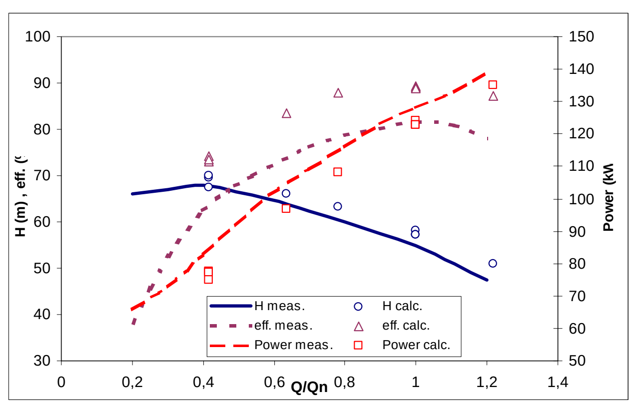

Figure 11 : Head, efficiency and power

The calculations show that the losses in the impeller and in the volute are both minimum at Qn. Additional losses occur at low flow where a recirculation is present, extending towards the inlet on ½ a diameter at 0.64 Qn and 3 diameters at 0.43 Qn (Figure 12)

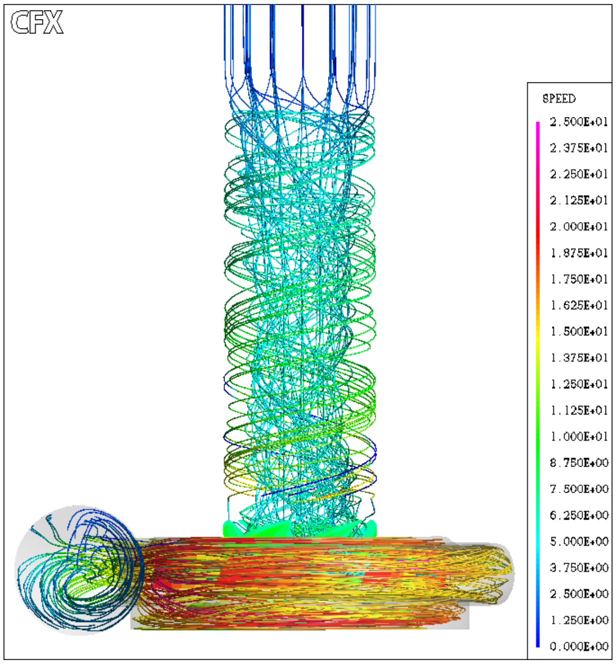

Figure 12 : Streamlines at 0.43 Qn

Flow description

The flow in the impeller is highly dependent of the flow rate. At nominal and high flow, one can notice a small recirculation zone on the hub along the suction side of the blade. At low flow, a large recirculation zone appears at the shroud along the pressure side, which extends backwards in the inlet pipe (figure 12).

At the impeller exit, the radial velocity is twice as high near the shroud than near the hub at nominal and high flow while it is more balanced at low flow. At 0.43 Qn, some outlet recirculations are locally present. The impeller exit pressure distribution depends also on the flowrate as can be seen on figures 15 to 17 : the pressure and suction sides of the volute are inverted.

Figures 13 and 14 show the streamlines in the volute casing at two flowrates, highlighting the difference of incidence at the tongue. Swirling structures are visible all along the outlet pipe downstream the volute casing.

Influence of the coupling model

At Qn and 0.43 Qn, flow simulations were done for three positions using the frozen rotor model and with the full unsteady model.

At Qn, some differences appear between the results at the three positions essentially in the pressure field close to the tongue (figures 13 and 14). The velocity fields are quite similar such as the pressure evolution on both sides of the blade. The overall performances (fig. 11) and the radial thrust (fig. 19) are not much influenced.

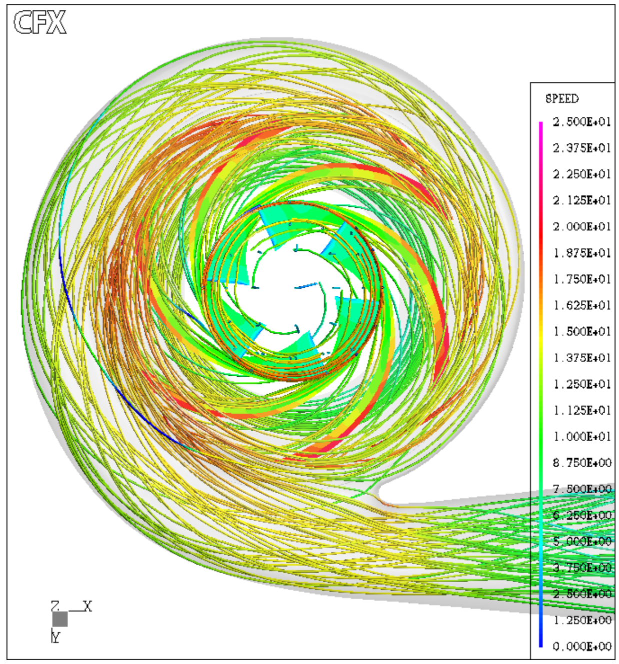

Figure 13 : Streamlines at Qn

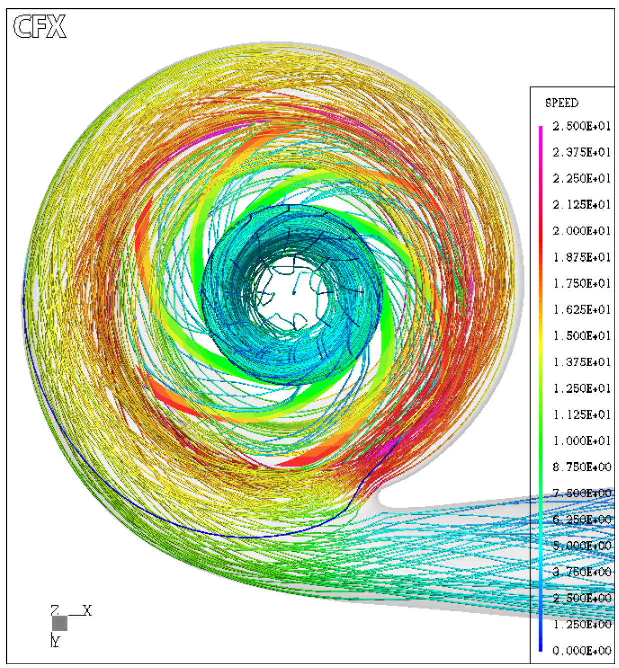

Figure 14 : Streamlines at 0.43 Qn

At low flow, the differences are more visible on the velocity and pressure fields and on the overall performances. The radial thrust in position 3 where a blade leading edge is in front of the tongue is 2.4 times higher than in position 2.

The unsteady calculations provide velocity and pressure fields similar to those obtained with the frozen rotor model. However pressure fluctuations due to the interaction between the blades and the volute tongue are noticeable in the whole flow domain, from the leading edge of the blades to the outlet pipe. They induce a fluctuating torque and power with at nominal flow an amplitude of 2% and a mean level 2% higher than those obtained with the frozen rotor model (figure 9).

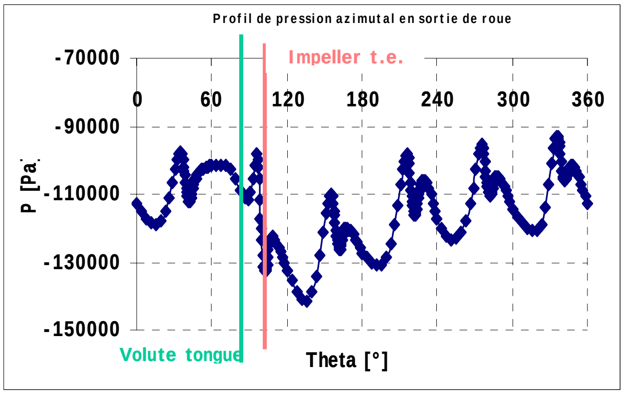

Figure 15 : pressure at the impeller outlet – Qn, position 1

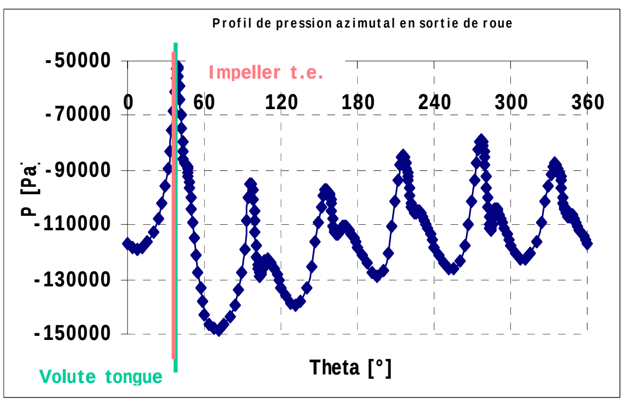

Figure 16 : pressure at the impeller outlet – Qn, position 3

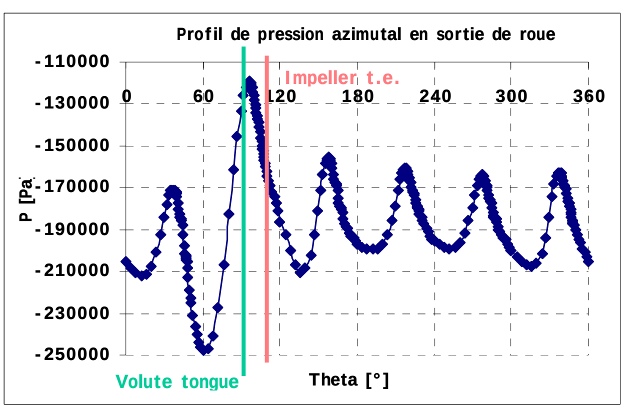

Figure 17 : pressure at the impeller outlet – 0.43 Qn, pos. 1

At low flow, the unsteady model shows less variations than the frozen rotor one. This fluctuating level is rather low due to the important radial gap between the impeller exit and the volute tongue, because of the trimming of the blades.

Radial thrust

As the balancing holes were not taken into account in the model, the computed axial thrust is not representative and will not be dealt with in this paper.

Figure 18 shows the orientation of the radial thrust for the 5 flowrates. At low flow, the thrust is oriented towards the exit while it is the opposite at nominal flowrate. On figures 19 and 20 are plotted the magnitude and the angle of the thrust compared to the experimental values.

The first curve presents the classical V-shape with the special feature that the minimum flowrate Qv is much less than the BEP flowrate Qn. The evolution of the magnitude of the radial thrust is in a good accordance with the measured one. At low flow, there is a large dispersion for the frozen rotor calculations.

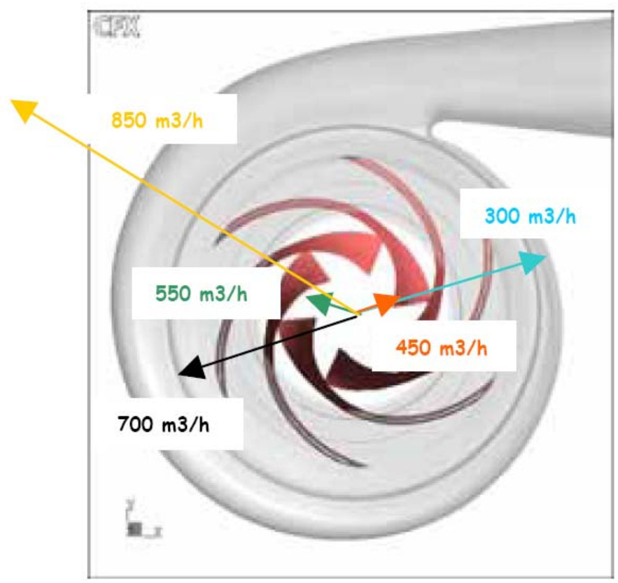

Figure 18 : Orientation of the radial thrust

On figure 20 the transition between both directions is more progressive in the experiment. The evolution of the angle at high flow is also different : the calculations show a decrease of the angle while it increases in the experiment.

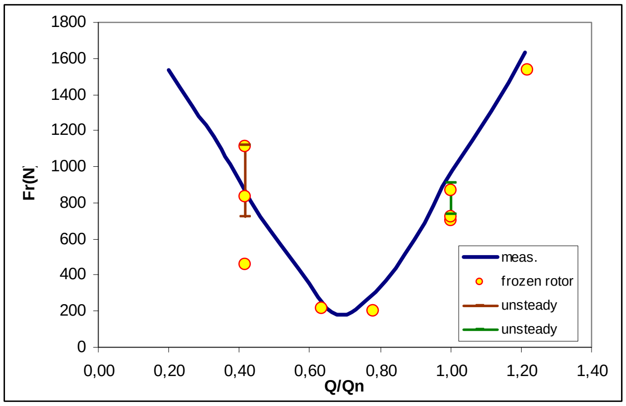

Figure 19 : Radial thrust

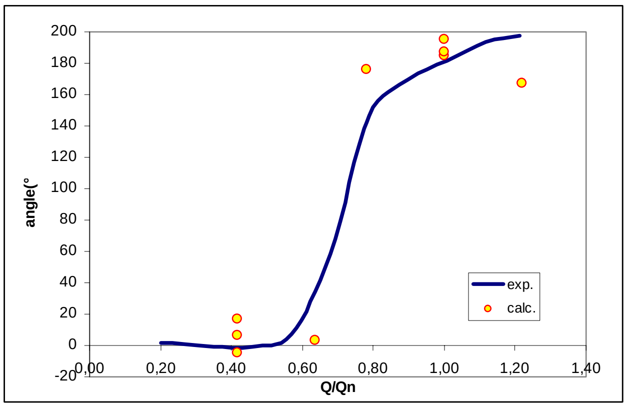

Figure 20 : Angle of the radial thrust

CONCLUSIONS

The radial thrust in a centrifugal pump has been determined both experimentally and numerically on a wide range of flow conditions. The measurements have been done owing to the development of a specific bearing allowing the measurement of axial and radial forces and moments and their fluctuations.

The numerical study was performed in order to check the ability of modern CFD codes to bring reliable information on the hydrodynamic forces exerted on the impeller. A 3D calculation of the whole pump including the impeller and the volute casing is necessary. For the tested pump, both frozen rotor and full unsteady model allowed to predict a correct evolution of the radial thrust and of its orientation.

REFERENCES

Asuaje M., Bakir F., Kouidri S., Kenyery F., Rey R., Numerical Modelization of the Flow in Centrifugal Pumps: Volute Influence in Velocity and Pressure Fields, Int. Journal of Rotating Machinery 2005(3) 244-255, 2005

Baun D.O., Flack R.D., Radial Impeller Forces using CFD, Part I : Model Development and Validation, ASME GT-2002-30377

Baun D.O., Flack R.D., Effects of Volute design and Number of Impeller Blades on Lateral Impeller Forces and Hydraulic Performance, Int. Journal of Rotating Machinery 9(2) 145-152, 2003

Chantrel P., Perret R., Boyer A., Development of a Conical Hydrostatic Bearing for Measuring Axial and Radial Forces on Pump Shafts, VDMA Pump Users Intl. Forum, 2004

Gonzalez J, Santolaria C., Blanco E., The effect of the volute tongue on the pressure oscillations inside a centrifugal pump, XXIst IAHR Symposium on Hydraulic Machinery and Systems, Lausanne, sept. 2002

Gülich J.F., Kreiselpumpen, Ein Handbuch für Entwicklung, Anlagenplanung und Betrieb, Springer, 1999

Kaupert K.A., A Computational Evaluation of Impeller Blade Moment, ASME FEDSM 2002-31200

Majidi K., Siekmann H.E., Numerical Calculation of Secondary Flow in Pump Volute and Circular Casings using 3D Viscous Flow Techniques, Int. Journal of Rotating Machinery 6(4) 245-252, 2000

Treutz G., Hansen T., Comparison of Steady-State and Transient Calculations of a Radial Pump Flow Field, XXIst IAHR Symposium on Hydraulic Machinery and Systems, Lausanne, sept. 2002